J Membrane Biol (2015) 248:1043–1060
DOI 10.1007/s00232-015-9816-7

HCN Channel C-Terminal Region Speeds Activation Rates Independently of Autoinhibition

Kaylee E. A. Magee[1] · Zarina Madden[1] · Edgar C. Young[1]

Received: 15 December 2014 / Accepted: 8 June 2015 / Published online: 30 June 2015

Abstract Hyperpolarization- and cyclic nucleotide-activated (HCN) channels contribute to rhythmic oscillations in excitable cells. They possess an intrinsic autoinhibition with a hyperpolarized $V_{1/2}$, which can be relieved by cAMP binding to the cyclic nucleotide binding (CNB) fold in the C-terminal region or by deletion of the CNB fold. We questioned whether $V_{1/2}$ shifts caused by altering the autoinhibitory CNB fold would be accompanied by parallel changes in activation rates. We used two-electrode voltage clamp on *Xenopus* oocytes to compare wildtype (WT) HCN2, a constitutively autoinhibited point mutant incapable of cAMP binding (HCN2 R591E), and derivatives with various C-terminal truncations. Activation $V_{1/2}$ and deactivation $t_{1/2}$ measurements confirmed that a truncated channel lacking the helix αC of the CNB fold (ΔαC) had autoinhibition comparable to HCN2 R591E; however, ΔαC activated approximately two-fold slower than HCN2 R591E over a 60-mV range of hyperpolarizations. A channel with a more drastic truncation deleting the entire CNB fold (ΔCNB) had similar $V_{1/2}$ values to HCN2 WT with endogenous cAMP bound, confirming autoinhibition relief, yet it surprisingly activated slower than the autoinhibited HCN2 R591E. Whereas CNB fold truncation slowed down voltage-dependent reaction steps, the voltage-independent closed-open equilibrium subject to autoinhibition in HCN2 was not rate-limiting. Chemically inhibiting formation of the endogenous lipid PIP_2 hyperpolarized the $V_{1/2}$ of HCN2 WT but did not slow down activation to match ΔCNB rates. Our findings suggest a "quickening conformation" mechanism, requiring a full-length CNB that ensures fast rates for voltage-dependent steps during activation regardless of potentiation by cAMP or PIP_2.

Keywords HCN channels · Autoinhibition · Two-electrode voltage clamp · Kinetics · Voltage-gating · PIP_2

Introduction

Hyperpolarization- and cyclic nucleotide-activated (HCN) channels respond to membrane hyperpolarization by producing an inward mixed Na^+ and K^+ current termed I_f, I_q, or I_h [see reviews (Kaupp and Seifert 2001; Robinson and Siegelbaum 2003)]. Deviations in HCN expression or function can contribute to several disease states (Benarroch 2013), including cardiac arrhythmias (Stieber et al. 2004), epilepsy (Noam et al. 2011) and neuropathic pain (Jiang et al. 2008). There are four mammalian genes encoding HCN subtypes (HCN1–HCN4), and in vivo HCN channels typically include at least two subtypes. They are notably regulated allosterically by the direct binding of cAMP, which causes a positive shift in the $V_{1/2}$ value (the voltage at which channels are activated to 50 % of their maximum), increases the speed of activation, and decreases the speed of deactivation (DiFrancesco and Tortora 1991; DiFrancesco 1999). Even in cells under basal conditions the endogenous level of cAMP may be high enough to influence HCN channel activity (DiFrancesco and Tromba 1988; Wang et al. 2002). HCN channels have been called "pacemaker" channels because of their function in

Electronic supplementary material The online version of this article (doi:10.1007/s00232-015-9816-7) contains supplementary material, which is available to authorized users.

✉ Edgar C. Young
youngec@sfu.ca

[1] Department of Molecular Biology and Biochemistry, Simon Fraser University, 8888 University Drive, Burnaby, BC V5A 1S6, Canada

oscillatory potentials, contributing to the spontaneous diastolic depolarization of the pacemaking sino-atrial node in the heart (Stieber et al. 2004; Mangoni and Nargeot 2008) and to rhythmic activity in the thalamus (Lüthi and McCormick 1998). Rhythmic oscillation relies on the dynamic responses of interdependent ion currents, so it is important to understand the structural features that influence the kinetics of the activation–deactivation cycle in HCN channels.

HCN channels have structural properties resembling classical voltage-gated K^+ channels (reviewed in Biel et al. 2009), including: tetrameric assembly; the presence in each subunit of six helical transmembrane segments arranged in a voltage-sensing domain (S1–S4) and a potassium pore domain (S5–S6); a pore gate formed by the cytoplasmic C-terminal end of S6 (Rothberg et al. 2002; Flynn and Zagotta 2003); and sensing of voltage by the positively charged S4 segment that moves inward upon hyperpolarization in the rate-limiting step for activation (Männikkö et al. 2002; Bell et al. 2004; Bruening-Wright et al. 2007). However, in HCN channels the coupling between S4 movement and gate-opening is reversed in direction from that of classical depolarization-gated channels, and is allosteric or loose (Altomare et al. 2001) rather than obligatory in the Hodgkin–Huxley tradition. In fact, for at least one subtype, HCN2, the gate-opening step is voltage-independent (Craven and Zagotta 2004; Chen et al. 2007). After initial gate-opening, the open state can be stabilised by a secondary conformational change, so that the depolarization-dependent deactivation pathway is not a reversal of the activation pathway (Männikkö et al. 2005; Elinder et al. 2006; Bruening-Wright and Larsson 2007; Wicks et al. 2009, 2011).

All HCN subtypes have following the S6 segment a distinctive large cytoplasmic C-terminal region including sequentially a C-linker, a cyclic nucleotide binding (CNB) fold, and an "extreme-C" region. In the absence of cAMP, the HCN channel is believed to be in an "autoinhibited" state, since removing the CNB fold by proteolysis or gene truncation (Barbuti et al. 1999; Wainger et al. 2001) has a potentiating effect similar to that of cAMP binding; an HCN channel truncated to remove the CNB fold is thus viewed as a minimal unit supporting fully uninhibited voltage-gating function (Wainger et al. 2001; Vemana et al. 2004). The presence of the N-terminal subregion of the CNB fold up to helix αB is sufficient to impose autoinhibition, whereas the final helix αC is necessary for cAMP-mediated relief of the autoinhibition (Wainger et al. 2001). Structural studies of soluble fragments of the C-terminal region have identified cAMP contacts in the CNB fold and conformational changes triggered by cAMP binding (Zagotta et al. 2003; Zhou and Siegelbaum 2007; Akimoto et al. 2014; Puljung et al. 2014) and demonstrated allosteric coupling of cAMP binding to tetrameric self-association of the C-linker (Zhou et al. 2004; Lolicato et al. 2011; Chow et al. 2012) [but see an opposing view (Craven and Zagotta 2004; Craven et al. 2008)]. Presumably rearrangement of the C-linker due to loss of cAMP from the CNB fold causes autoinhibition by inducing a strain on the S6 pore gate, hence destabilising the open state relative to the closed state. This structural model focused on S6 and the C-linker provides a straightforward prediction of how autoinhibition regulates the thermodynamics of the gate-opening closed-to-open step, but it is less straightforward to predict how autoinhibition regulates the kinetics of voltage-dependent activation governed by the transmembrane S4 segment.

One possibility is that the autoinhibition and relief mechanisms would simply modify kinetics parallel to the modifications in $V_{1/2}$ values; that is, relief conditions that produce depolarized $V_{1/2}$ values would produce faster activation, while autoinhibition conditions that produce hyperpolarized $V_{1/2}$ values would produce slower activation. But the thermodynamic and kinetic effects of autoinhibition in principle are not constrained to be parallel, depending on the particular nature of the transition state in question. And if a different gating step is rate-limiting (not the steps regulated by autoinhibition), then autoinhibition may have no effects on the activation kinetics at all.

In this study, we set out to clarify whether the prevailing model of CNB fold-mediated autoinhibition would suitably describe gating kinetics of HCN2 channels. To ensure we knew the exact composition of our tetramers we heterologously expressed HCN channel derivatives as homomers in intact *Xenopus* oocytes (Chen et al. 2000, 2001; Santoro et al. 2000; Wang et al. 2002). Specifically, we sought to test the notion that the thermodynamics and kinetics should be regulated in a parallel fashion: Does the introduction of an intact unliganded CNB fold slow activation kinetics in parallel to its known effect of hyperpolarizing $V_{1/2}$ values? As autoinhibition can also be imposed by introducing only the N-terminal subregion of the CNB fold, would this introduction equally induce slow activation kinetics? Does speeding of deactivation accompany the slowing of activation due to autoinhibition? Does the voltage-independent gate-opening step of HCN2 restrict the activation rate in autoinhibited channels, and are these kinetic restrictions removed when autoinhibition is relieved by CNB fold deletion? Our findings suggest that any slowing effect of autoinhibition on activation kinetics must be restricted to steps that are not rate-limiting, and suggest there is an additional mechanism which can preserve a high rate of activation only when the full CNB fold sequence is present. This new mechanism accounts for a kinetic difference between channels whose autoinhibition is relieved in different ways: by CNB fold deletion or by addition of cAMP.

Our new mechanism does not contradict autoinhibition, but introduces an additional element to consider when examining channel activation speeds to further characterise the gating of the HCN channel family.

Materials and Methods

Composition and Subcloning of DNA Constructs

All channels in this investigation were subcloned into the high-expression vector pGEM-HE (Liman et al. 1992) to allow in vitro transcription of RNA from linearized DNA with the T7 promoter (Ambion mMessage Machine Kit). All channels were expressed in *Xenopus* oocytes (see below) as homomers. "HCN2" or "HCN2 WT" in this report denotes full-length wild-type mouse HCN2 (863 amino acids) (Ludwig et al. 1998). The HCN2 R591E derivative (Chen et al. 2001) is identical to HCN2 with the exception of the Arg to Glu mutation at residue 591. Composition of deletion derivatives were as follows: ΔXC consists of HCN2 amino acids 1-645, previously reported as "HCN2 Δ645"(Zagotta et al. 2003); ΔαC consists of HCN2 amino acids 1-617, previously reported as $HCN2_{\Delta C\text{-}\alpha}$ (Wainger et al. 2001); ΔCNB consists of HCN2 amino acids 1-525, previously reported as $HCN2_{\Delta CNBD}$ (Wainger et al. 2001). HCN2, HCN2 R591E and ΔCNB were generous gifts from S. A. Siegelbaum, ΔXC had been previously constructed by E. C. Y. and ΔαC was reconstructed by K. E. A. M. using PCR mutagenesis. Regions of constructs which were involved in PCR mutagenesis during construction of these clones were verified by us using dideoxy sequencing (Eurofins Operon).

TEVC Recordings

Oocytes were obtained through ovariectomies of *Xenopus laevis* frogs following guidelines from the Canadian Council on Animal Care. Oocytes were then defolliculated by collagenase (Sigma Aldrich) as previously reported (Wicks et al. 2009) and washes after collagenase treatment used either ND96 (Cedar Lane Laboratories) or "Magnesium Oocyte Ringer 2" (in mM: 96 NaCl, 2 KCl, 20 $MgCl_2$, 5 HEPES, pH 7.4), either of which was then followed by "Oocyte Ringer" (in mM: 1.8 $CaCl_2$, 2 KCl, 115 NaCl, 10 HEPES, pH 7.3). Both before and after RNA injection, oocytes were stored at 16 °C in Barth's Saline solution (Modified without Ficol 400, Cedar Lane) with 100 ng/μL of the antibiotic gentamicin (Sigma Aldrich) with at least one daily change to fresh solution after injection. Oocytes were injected with 15–40 ng channel RNA within 24 h of collagenase treatment, and recordings were obtained 3–4 days after injection.

TEVC recordings reported in this work were generated from the oocytes of at least two frogs for each channel type or condition, and each batch of oocytes extracted for this study was used for testing at least two channel types or conditions. Thin-walled glass capillaries with filaments (World Precision Instruments Category # TW150F-3) were pulled to form TEVC electrodes with a resistance between 0.2 and 2.2 MΩ when filled with 3 M KCl. TEVC experiments were completed at room temperature (19–23 °C) using a GeneClamp 500B amplifier and Digidata 1440A (both Axon Instruments) and the computer program Clampex 10.2. Current was filtered at 1 kHz and sampled at 10 kHz; datapoints have been undersampled in Figures for clarity of printing. The TEVC Bath solution consisted of (in mM): 96 NaCl, 3 KCl, 5 HEPES (pH 7.4), 1 $MgCl_2$, 0.75 $CaCl_2$. For Wortmannin treatments, a stock solution of 30 mM Wortmannin (Sigma) was prepared in DMSO and stored at −20 °C; this stock solution (or an equal volume of DMSO alone) was then diluted into TEVC Bath to produce a 45 μM Wortmannin test solution, with maximum 6 h wait before application. Wortmannin effects were measured by first recording from the oocyte in TEVC Bath without Wortmannin, then removing the electrodes and incubating the oocyte in the 45 μM Wortmannin test solution for 35 min, then returning to TEVC Bath without Wortmannin for immediate re-impalement and recording. The 45 μM Wortmannin concentration was deemed saturating since trials with 120 μM did not produce appreciably greater hyperpolarizations of $V_{1/2}$.

Voltage clamp holding potential was −40 mV and oocytes were excluded from analysis if they exhibited inward leak current greater than 200 nA at this voltage. The activation protocol (Online Resource 1) included a hyperpolarizing activation epoch (−40 mV to −170 mV, every 10 mV) followed by a tail epoch (−120 mV) and a deactivation epoch (+20 mV). A "staircase" of steps to +40, 0, and −40 mV was applied at the end of every sweep, to verify stability of time-independent currents. Channel behaviour was stable for tens of minutes, judged by reproducibility of repeated recordings.

At the beginning of the activation epoch, a small lag segment with concave negative shape consistently occurred in the trace, with an inflection point leading to the concave positive activation transient as reported previously for HCN currents (DiFrancesco 1999; Wainger et al. 2001). In some recordings, time-dependent currents not typical of HCN channel behaviour were observed in the later portion of the activation epoch, with either a decrease in inward current ("sag") or a second inflection point leading to concave negative curvature ("post-plateau instability"). These behaviours were not systematically observed but occurred more often at −150 mV or more negative (see Online Resource 1 for examples at −170 mV). Oocytes

were excluded from analysis altogether if either of these behaviours occurred at −130 mV or less negative; additionally, individual sweeps at −150 mV or beyond were excluded if either behaviour appeared within the first 800 ms of activation.

Analysis

For determining $V_{1/2}$, tail current values at −120 mV were measured using Clampfit 10.2 at the local peak following the capacitance clearance (typically < 25 ms). Using Sigmaplot 10.0, activation voltages (V) and tail current values (I) were fit to the four parameter sigmoid Boltzmann equation $I = y_0 + a/(1 + \exp[-(V - V_{1/2})/s])$. The floating parameters were a (positive, maximum time-dependent HCN current amplitude), s (positive, reciprocal slope), $V_{1/2}$ (negative, midpoint activation voltage) and y_0 (negative, total maximum current), from which the I_{leak} parameter (negative, "leak" current) was calculated as $I_{leak} = (y_0 + a)$. I_{leak} includes both the instantaneous component of HCN conductance (Proenza et al. 2002) and non-HCN sources of leak; the average value of $|I_{leak}|/a$ for each channel type was in the range 0.02–0.08, so we can conclude that a majority of HCN current observed from our channels was time-dependent HCN current. As described below, in many cases and especially for HCN2 and ΔXC which can bind endogenous cAMP, the absolute inward current did not reach a steady state during the activation epoch (see Online Resource 1 for typical recordings). Thus, our isochronal tail currents generally underestimate the steady-state conductance levels, which limits the precision of the estimates of $V_{1/2}$ and s.

For kinetics of the activation epoch, the concave negative lag segments, as well as portions of traces at −150 mV showing sag or post-plateau instability, were truncated to isolate concave positive datasets for exponential fitting. Activation tau (τ) values were determined using Clampfit 10.2 by Levenberg–Marquardt fitting of each activation trace to the double exponential equation $I(t) = A_{early} \exp[-t/\tau_{early}] + A_{late} \exp[-t/\tau_{late}] + C$, where $\tau_{early} < \tau_{late}$. Amplitudes ($A_i$) and time constants ($\tau_i$) were forced positive on all fits. For quantitation of the lag duration, d, an iterative fitting procedure based on Wicks et al. (2009) was used. An initial overestimate of d was made that encompassed some of the early concave positive region, and fitting was done using only time points after the overestimated d. Then the earliest time point before d exhibiting good match to the fit curve was found by visual inspection, and this became the new smaller estimate of d. Fitting and reduction of d was then repeated until d could no longer be reduced without compromising fit quality.

We judged that two exponential terms were generally sufficient because the fit residual R = (sum of squared errors)/(sum of data squared) for −130 mV activation traces improved significantly when the number of terms was increased from one to two, but improved markedly less upon addition of a third term, with no difference in fit quality on visual inspection (Online Resources 3, 4). Although double exponential fitting was applied in all cases, some traces (particularly at voltages −90 to −110 mV) have only τ_{early} reported, for the following reasons: In some cases, one component was insignificant with $A_i/(A_{early} + A_{late}) < 0.03$, indicating a single exponential was sufficient. In other traces, the τ_{late} was >10 s, indicating a quasi-linear component. Because traces did not all reach endpoint, the fractional contribution of the early component to total activation trace amplitude (f_{early}) was calculated over the fitted time interval (Δt) as $f_{early} = A_{early} \exp[-\Delta t/\tau_{early}]/\{A_{early} \exp[-\Delta t/\tau_{early}] + A_{late} \exp[-\Delta t/\tau_{late}]\}$.

The deactivation protocol (Online Resource 8) contained an activation epoch (−140 mV) followed by a deactivation epoch of either +40, +20, or 0 mV. Because deactivation currents always reached a steady endpoint, kinetics were quantified by a $t_{1/2}$ value, determined as the time required to reach the midpoint of deactivation current (starting from the beginning of the deactivation epoch). Starting (lag plateau) values of current were visually identified following capacitance clearance (<25 ms). Oocytes for which the $V_{1/2}$ value and activation τ calculations were both excluded were also removed from our deactivation $t_{1/2}$ dataset.

Mean values are reported ±SD with number of determinations indicated by n. Comparisons of mean values were assessed by one-sided t test (to detect an inhibitory effect) or two-sided t test (to detect a difference) with a significance threshold of $p = 0.05$.

Results

Two Constitutively Inhibited HCN2 Derivatives Exhibit Different Kinetics

We used the *Xenopus* oocyte expression system with two-electrode voltage clamp (TEVC) to record hyperpolarization-activated currents from homomeric mouse HCN2 channels and HCN2 derivatives (Fig. 1 upper panels; Online Resource 1). Autoinhibition relief in full-length HCN channels requires not only cAMP binding but also conformational changes, so there should be a variety of ways to disrupt the relief mechanism. We hypothesised that, based on the autoinhibition model, changes to the C-terminal region should influence thermodynamics and kinetics in a parallel manner. This hypothesis predicts that regardless of how autoinhibition relief is disrupted, fully

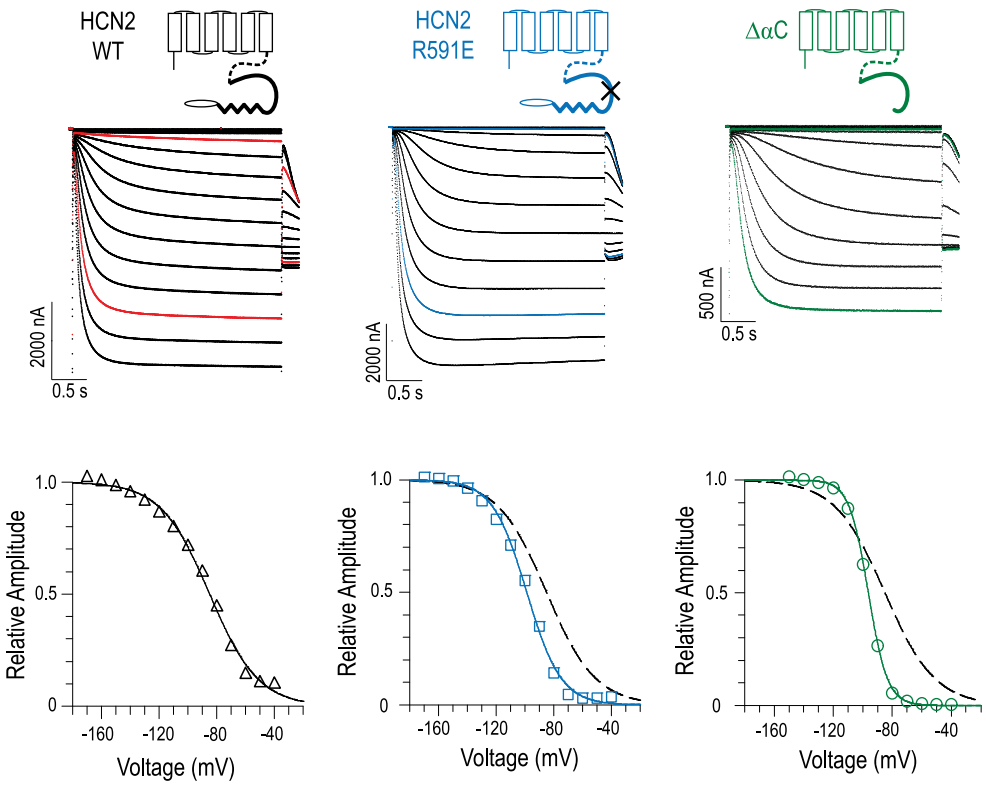

Fig. 1 Two mutant HCN2 derivatives exhibit constitutive autoinhibition in intact oocytes. *Upper panels* show representative examples of hyperpolarization-activated inward currents of mouse HCN2 WT and mutant derivatives. Subunit structures are depicted in schematic icons including subregions of C-terminal region: C-linker (*dashed line*), CNB fold (*bold line*) including helix αC (*zigzag*) and extreme-C region (*oval*); R591E point mutation is shown with a *cross*. Channels were expressed in *Xenopus* oocytes and studied using two-electrode voltage clamp; only activation and tail epochs are shown, and the −160 and −170 mV traces of ΔαC were excluded due to post-plateau instability (see "Materials and Methods" and Online Resource 1 for protocol and example traces in full). Traces for −70 and −150 mV activation are highlighted for clarity. *Lower panels* show conductance–voltage relations from tail currents (*points*, data from corresponding upper panels) after correction by leak-subtraction and normalisation to maximal amplitude determined from a Boltzmann equation fit (*solid curves*, see "Materials and Methods"). For comparison, the example HCN2 WT curve is repeated as a *black dashed line* in the panels of mutant derivatives. Boltzmann equation fit parameters were as follows: HCN2 WT, $V_{1/2} = -84.9$ mV, $s = 16.9$ mV; HCN2 R591E, $V_{1/2} = -98.7$ mV, $s = 11.9$ mV; ΔαC, $V_{1/2} = -96.2$ mV, $s = 6.48$ mV. See Online Resource 7a for mean values

autoinhibited channels should show identical kinetic behaviours. We sought to test this hypothesis in intact oocytes by comparing two examples of HCN2 derivatives with constitutive autoinhibition imposed in two different ways. Previous TEVC studies have examined HCN2 R591E, which has its autoinhibitory CNB fold mutated to remove the positively charged arginine residue that contacts cAMP (Chen et al. 2001; Wang et al. 2002). We compared HCN2 R591E to the derivative ΔαC which has its CNB fold truncated (Fig. 1 upper right): the N-terminal "β-roll" moiety region of the CNB is still present [preserving the cAMP-contact arginine 591 (Zagotta et al. 2003)] and is sufficient to impose autoinhibition, but the truncation removes the helix αC which is critical for contacting cAMP during autoinhibition relief (Wainger et al. 2001; Zhou and Siegelbaum 2007).

Activation traces at weakly hyperpolarized voltages show evidence that activation is indeed inhibited in both HCN2 R591E and ΔαC compared to HCN2 WT in the presence of endogenous cAMP. For instance, for HCN2 WT the trace at −70 mV is the first to indicate an observable increase of inward current across the 3-s epoch, while this "threshold" activation does not appear in HCN2 R591E or ΔαC until −90 mV (Fig. 1 highlighted −70 mV curves). This suggests that HCN2 WT requires approximately 20 mV less hyperpolarization than HCN2 R591E or ΔαC to achieve comparable channel activation. This suggestion was quantitatively confirmed by the mean $V_{1/2}$ values recorded from the tail epoch in our activation protocol. The mean $V_{1/2}$ values of HCN2 R591E (−99.4 ± 3.1 mV, $n = 10$) and ΔαC (−101.1 ± 5.5 mV, $n = 10$) were both significantly more hyperpolarized (one-

sided $p < 10^{-5}$) compared to that of HCN2 WT (−83.4 ± 5.0 mV, $n = 49$; see Fig. 1 lower panels and Online Resource 7a for $V_{1/2}$ means). The $V_{1/2}$ values of the two autoinhibited channels were not significantly different from each other (two-sided $p > 0.3$). Our $V_{1/2}$ values matched previous reports [−80 mV for HCN2 WT (Zolles et al. 2006); −97 to −102 mV for HCN2 R591E (Chen et al. 2001; Wang et al. 2002)] and are consistent with HCN2 R591E and ΔαC possessing similarly strong autoinhibition which is constitutive, i.e. it is not relieved by endogenous cAMP.

The hypothesis of parallel thermodynamic and kinetic effects implies that the autoinhibited HCN2 R591E and ΔαC with similar $V_{1/2}$ values should have similar slow activation kinetics. Surprisingly contrary to this prediction, these two channels did not exhibit identical kinetic behaviour; rather, superimposition of traces at the same voltage suggested that activation was perceptibly slower for ΔαC than HCN2 R591E (Fig. 2 left panels). After exclusion of an initial concave negative lag period (*d*), HCN2 R591E and ΔαC transients at −90 mV were fitted well to a single exponential curve as previously noted for HCN2 R591E (Wang et al. 2002). Although a double exponential fit was more suitable at stronger hyperpolarizations (see next paragraph), we confirmed that the quantitation outcome for −90 mV transients did not substantially change upon introducing a second exponential component for fitting, because the faster "early" component represented almost the entire fit—its relative contribution to decay amplitude (f_{early}) was almost 1 (see Fig. 2, fits at −90 mV). Moreover, the time constant for the slower "late" component (τ_{late}) grew markedly longer as hyperpolarization grew weaker, so that even if this late component had detectable amplitude, its time course was so slow as to be nearly linear (see Online Resource 2 for f_{early}, τ_{late} data). At −90 mV, the time constant for the dominant early component (τ_{early}) was 1710 ± 380 ms ($n = 9$) for ΔαC, which was over 2.2-fold slower than τ_{early} for the comparably autoinhibited HCN2 R591E (760 ± 240 ms, $n = 10$).

We extended our comparison of autoinhibited channels to stronger hyperpolarizations, as different mechanistic steps may be rate-limiting at different voltages. Again, ΔαC opened significantly slower than HCN2 R591E. For both derivatives, a double exponential fit was superior to a single exponential fit at stronger hyperpolarizations (Fig. 2, fits at −130 mV; Online Resource 3) which might reflect slow formation of secondary open states after the initial fast closed-open transition (Altomare et al. 2001).

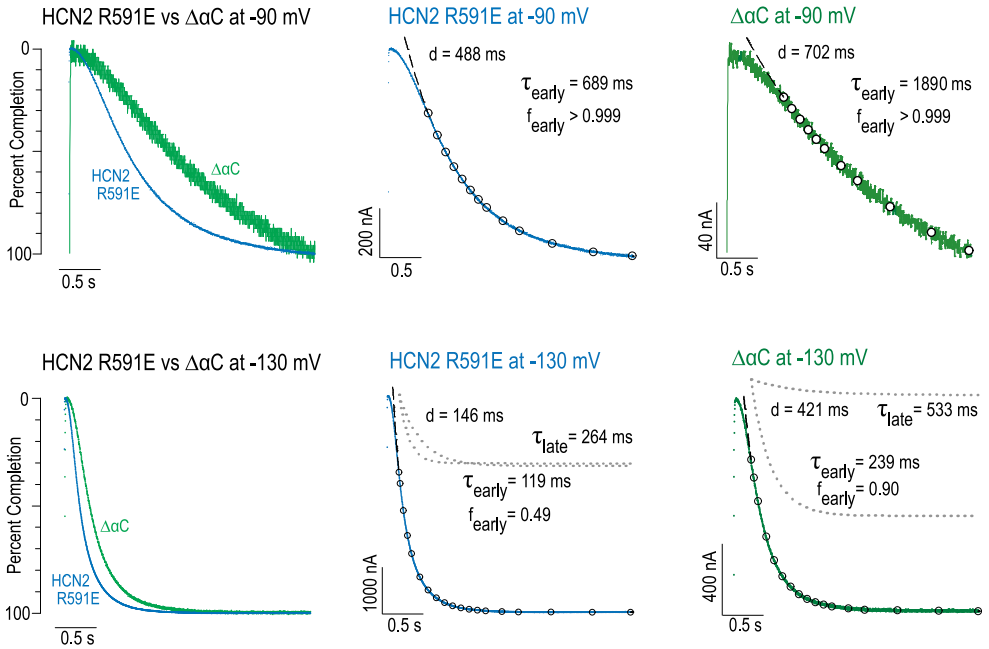

Fig. 2 Two constitutively autoinhibited HCN2 derivatives exhibit different activation kinetics. *Left panels* show superimpositions of representative activation transients of each derivative at indicated voltages. Transients have been normalised to the total decay amplitude observed over the 3-s activation epoch. *Middle and right panels* show double exponential fits for activation transients from corresponding *left panels*. Current datapoints are shown as *points*; *open circles* show currents calculated at selected times for the fitted decay equation. Extension of fitted equation to times before the fit boundary is shown by *dashed curves*. For −130 mV traces, *dotted grey curves* show individual components of the double exponential fit, with an arbitrary vertical offset for clarity. Lag duration (*d*), time constants (τ_{early} and τ_{late}) and fractional contribution of the earlier component (f_{early}) are indicated; note late components at −90 mV are negligible

However, the early component accounted for the majority of activation transient amplitudes (mean $f_{early} > 0.5$ for all derivatives in this study at all voltages), so we focused on this parameter for all future kinetic comparisons. The mean τ_{early} for ΔαC was slower than that of HCN2 R591E by a factor of >1.5-fold at all voltages studied (one-sided $p < 0.001$, for −90 mV through −150 mV; Fig. 3). There was also a noticeable lengthening of the lag duration d in ΔαC by a factor of >1.3-fold compared to HCN2 R591E at hyperpolarizations −110 mV and more negative (one-sided $p < 0.002$ for all voltages except −90 mV).

Thus, while the different modifications of the C-terminal region produce autoinhibition to a similar degree as indicated by $V_{1/2}$ in ΔαC and HCN2 R591E, the two inhibition mechanisms are not exactly coincident, because only HCN2 R591E is capable of a relatively fast response to hyperpolarization (e.g. $\tau_{early} < 100$ ms at −150 mV and <1 s at −90 mV; Fig. 3).

A previous study (Wang et al. 2002) showed time constants generally slower than ours for full length channels at comparable voltages, which suggests differences in bath solutions or endogenous levels of modulating factors in oocytes could lead to different rates for the same mechanism. Thus, we should exercise caution in comparing absolute numerical values of kinetic constants between studies. Rather, our hypothesis testing is based on comparisons between channels in one set of oocytes.

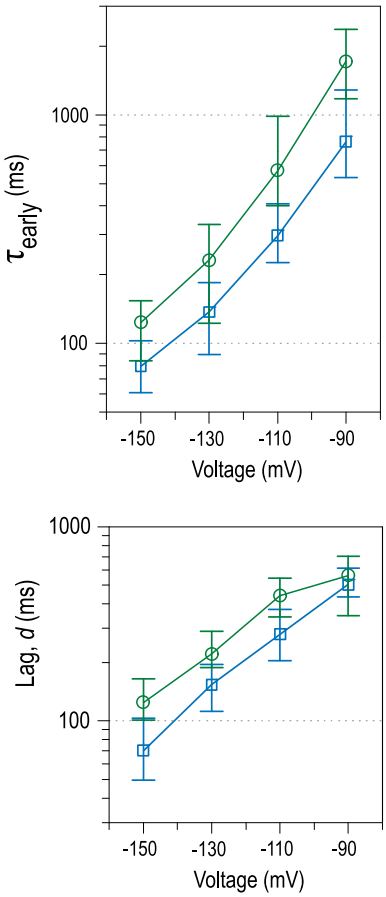

Fig. 3 Difference in early phase of activation between constitutively autoinhibited channels persists over a range of voltages. *Points* plot mean values of τ_{early} and d for HCN2 R591E (*blue squares*) and ΔαC (*green circles*). Error bars on log-axis plots show ranges of values. See Online Resource 2 for f_{early} and τ_{late} values characterising the minority late phase. For each derivative a total of 10 recordings were analysed, except that one transient of ΔαC at −90 mV was excluded because its total amplitude was <60 nA

The Helix αC But Not the Extreme-C Region is Necessary to Preserve a Fast Early Phase of Activation Similar to Unliganded Full-Length HCN2 Derivatives

The difference in kinetics of HCN2 R591E and ΔαC raises the issue of which one of these derivatives more accurately mimics the behaviour of an unliganded HCN2 WT channel. In one scenario, ΔαC could reflect the mechanism and kinetics of a full length unliganded HCN2 channel, and HCN2 R591E could possess a non-canonical structure and mechanism, due to its charge-reversing mutation, that made its activation faster than unliganded HCN2 WT. In an opposing scenario, HCN2 R591E could reflect the mechanism and kinetics of unliganded HCN2, and the presence of the helix αC or extreme-C region or both could be important for the channel to maintain a specific conformation enabling fast activation. This "quickening" conformation would be preserved in HCN2 R591E and unliganded HCN2 WT but would be compromised by truncation of the CNB fold in ΔαC. We favour this latter scenario based on comparison of our TEVC recordings of HCN2 WT and HCN2 R591E, as explained below.

HCN2 WT channels exist mostly in unliganded form during TEVC experiments, because the concentration of cAMP is low in the *Xenopus* oocyte as for other typical cells under basal conditions (DiFrancesco and Tromba 1988; Wang et al. 2002). Thus, when a strong hyperpolarization is applied to HCN2 WT in a TEVC recording, the early phase of the activation transient predominantly reflects the opening of unliganded channels, and substantial cAMP binding to accumulate liganded channels will occur only during a later phase (Online Resource 4). In contrast, when a weak hyperpolarization is applied to HCN2 WT, the activation rate of unliganded channels is slow enough that the observable activation transient is dominated by the minority population of cAMP-liganded channels with faster activation.

This contrast allows us to look for evidence of anomalously rapid activation of HCN2 R591E by comparing its early phase of activation to that of HCN2 WT (Online

Resource 4) specifically at strongly hyperpolarized voltages where both time constants reflect opening of unliganded channels. If the charge-reversing mutation in HCN2 R591E confers anomalously rapid activation, we would expect τ_{early} for HCN2 R591E to be faster than τ_{early} for HCN2 WT at the same strong hyperpolarization. However, we saw no evidence for such a rate difference. Instead, the τ_{early} of HCN2 R591E was not significantly faster than that of HCN2 WT at any voltages (one-sided $p > 0.08$, Online Resource 2). At −110 mV or weaker the τ_{early} of HCN2 R591E was significantly slower than that of HCN2 WT (one-sided $p < 0.009$), as expected since the HCN2 WT recordings at weak hyperpolarizations reflect cAMP-liganded channels. Overall, the comparison of early phases in activation of HCN2 WT and HCN2 R591E show no evidence for HCN2 R591E activating anomalously fast compared to unliganded HCN2 WT.

We further observed comparable τ_{early} values in another derivative, ΔXC, which lacks the extreme-C region but has an intact CNB fold along with arginine at position 591. The EC50 for cAMP binding to ΔXC is ~tenfold higher than for HCN2 WT (Chen et al. 2001; Zagotta et al. 2003). This strongly suggests a weaker overall cAMP affinity in ΔXC compared to HCN2 WT, so that ΔXC is even more likely than HCN2 WT to be unliganded at the low levels of endogenous cAMP in the oocyte. We found that ΔXC exhibited gating properties that were not noticeably inhibited relative to full length HCN2 WT (Online Resource 5). This included a similar $V_{1/2}$ (for ΔXC, −86.2 ± 9.2 mV, $n = 9$; not significantly more negative than for HCN2 WT, one-sided $p > 0.1$), and qualitatively similar biphasic activation kinetics. There was moreover no significant slowing found for any of the fitted gating parameters of ΔXC relative to HCN2 WT, one-sided $p > 0.2$ for all comparisons) including time constants of either the early or late components (τ_{early}, τ_{late}), and duration of the lag phase (d) (Online Resource 2). Even the fractional contribution of the early component (f_{early}) was not significantly different (two-sided $p > 0.07$, all voltages). This is consistent with both HCN2 and ΔXC being primarily in the unliganded state at the holding voltage preceding the activation epoch in our protocol.

Thus, ΔXC has an intact CNB fold and activates with a fast early phase (e.g. τ_{early} ~500 ms at −90 mV) whose dominant contribution is likely to be from unliganded channels resembling HCN2 R591E or unliganded HCN2 WT. But the fast response is significantly slowed on deletion of the helix αC (τ_{early} ~1700 ms at −90 mV). The helix αC can therefore be viewed as a critical element not only for relief of autoinhibition upon cAMP binding, but also for maintaining a "quickening" conformation that supports efficient activation kinetics when the channels are still unliganded.

Relief of Autoinhibition by Deletion of the CNB Fold Fails to Preserve the Fast Activation Kinetics of Full Length HCN2

Deleting the inhibitory CNB fold altogether should relieve autoinhibition and, if thermodynamic and kinetic effects are parallel, might be expected to speed up activation compared to that of intact autoinhibited channels; on the other hand, the loss of helix αC in such a deletion might be expected to prevent the quickening conformation and thus, slow down activation. To investigate the relative importance of autoinhibition and the quickening conformation for determining activation kinetics, we examined ΔCNB, the same derivative which was originally used to establish the autoinhibition model (Wainger et al. 2001); this derivative contains the C-linker but lacks the entire CNB fold and the extreme-C region.

ΔCNB had a mean $V_{1/2}$ value of −82.9 ± 7.4 mV ($n = 6$; Fig. 4a, b) which was significantly more positive than that of autoinhibited HCN2 R591E (one-sided $p < 0.002$) but not that of HCN2 WT (one-sided $p > 0.4$; see Online Resource 7a for summary of $V_{1/2}$ means). As with HCN2 R591E, activation transients of ΔCNB showed a late component (Fig. 4c) whose contribution decreased with progressively weaker hyperpolarizations, as distinct from the slow cAMP-dependent phase persisting at all voltages typical of HCN2 WT (Online Resources 2, 4). This confirms that as expected, ΔCNB had autoinhibition relieved in a manner different than HCN2 WT, in that it did not involve slow cAMP binding during the activation transient.

Despite the relief of autoinhibition, ΔCNB failed to show markedly faster kinetics compared to unliganded full-length channels HCN2 R591E and HCN2 WT (Fig. 4d to f, Online Resource 6). The mean τ_{early} of ΔCNB was significantly slower than that of the two full-length channels at all voltages (Fig. 4e, one-sided $p < 0.05$). The slowness of ΔCNB activation is especially remarkable considering that $V_{1/2}$ of ΔCNB is at least 15 mV more depolarized than that of the autoinhibited derivatives, indicating a stronger driving force for inward voltage-sensor movement in ΔCNB at a fixed voltage. This suggests that the removal of autoinhibition by deleting the CNB fold was insufficient to ensure fast activation kinetics. We propose that just as the loss of the helix αC in ΔαC compromised the "quickening conformation" of the intact CNB fold found in ΔXC, a similar distortion of conformation occurs upon deletion of the entire CNB fold to produce ΔCNB.

The effect on activation kinetics due to losing the quickening conformation appears similar in severity across a range of activation voltages. Comparing HCN2 WT and ΔCNB, which show similar $V_{1/2}$ values characteristic of relieved autoinhibition, the HCN2 WT channels with the

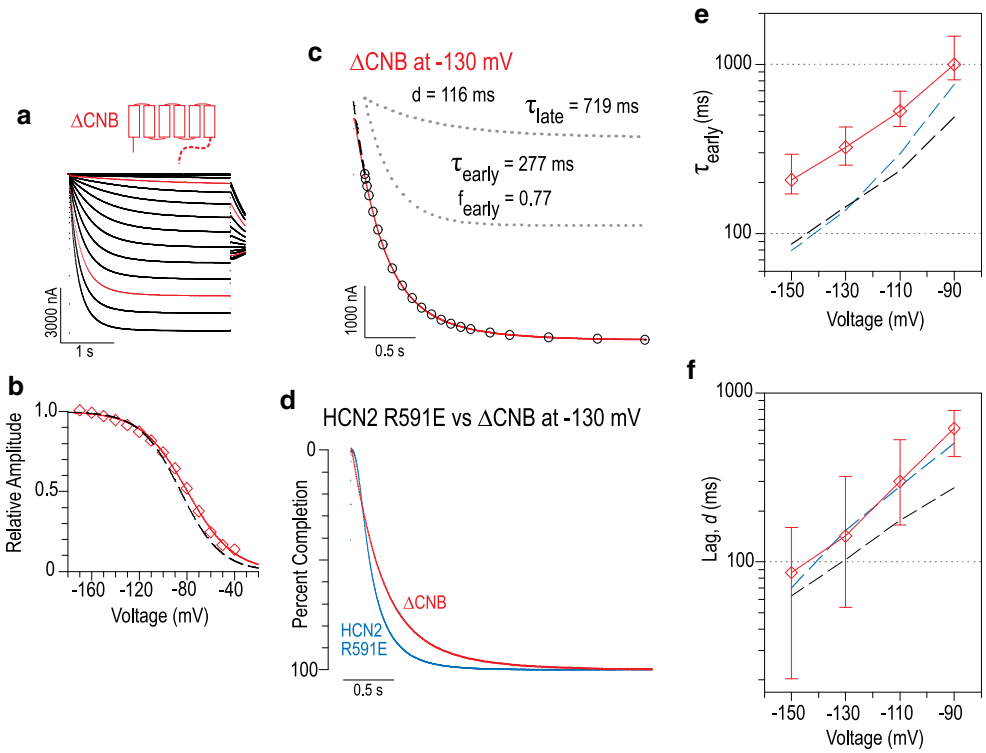

Fig. 4 Channel lacking the CNB fold exhibits slower activation than intact channels with or without cAMP binding. **a** Representative example of activation currents for ΔCNB with traces at −70 and −150 mV highlighted. Schematic icon at *top* shows truncated structure retaining only C-linker in C-terminal region. **b** Conductance–voltage relation from panel a formatted as in Fig. 1 (data *points* and *fitted solid curve*), including HCN2 WT relation for comparison (*dashed line*, from Fig. 1). Boltzmann equation fit parameters for ΔCNB were $V_{1/2} = -79.4$ mV, s = 19.2 mV. **c**, **d** ΔCNB activation transient at −130 mV with double exponential fit (**c**, formatted as in Fig. 2-right) and with superimposed HCN2 R591E transient (**d**, normalised as in Fig. 2-left). See Online Resource 6 for further example at −90 mV and comparison with HCN2 WT. **e, f** Mean parameters for early phase of ΔCNB activation (*points*, formatted as in Fig. 3; see Online Resource 2 for τ_{late} and f_{early}); a total of 6 recordings were analysed. For comparison, mean values are shown for HCN2 WT (*black dashed lines*) and HCN2 R591E (*blue dashed lines*) are shown (see Online Resource 2 for *error bars*)

quickening conformation had τ_{early} values at least twofold faster across all voltages studied from −90 to −150 mV (Fig. 4e). While we typically made comparisons between channel types at a fixed test hyperpolarization, the kinetic difference between channel types due to the quickening conformation is even more dramatic if we take the alternative approach of selecting test voltages a fixed difference from each channel's $V_{1/2}$ value. Thus, choosing a test voltage approximately 30 mV negative of $V_{1/2}$, the τ_{early} of HCN2 R591E at −130 mV (140 ± 30 ms, $n = 10$) is >3.8 times faster than the τ_{early} of ΔCNB at −110 mV (530 ± 100 ms, $n = 6$). The difference in activation speeds between ΔCNB and full-length derivatives is also sizable compared to the relatively shallow dependence of kinetics on activation voltage. The mean τ_{early} at −150 mV for ΔCNB is similar to τ_{early} at −110 mV for HCN2 WT (Fig. 4e); thus, truncating the CNB fold from an unliganded full-length HCN2 channel has roughly the same effect on kinetics as weakening the applied hyperpolarization by 40 mV. For comparison, we note that 40 mV is much larger than the approximately 20 mV positive shift in the $V_{1/2}$ that results from binding of cAMP to a full-length HCN2 channel (Wainger et al. 2001).

The Voltage-Independent Gate-Opening Step is Not Rate-Limiting, Whereas the Quickening Conformation But Not Autoinhibition Controls a Voltage-Dependent Rate-Limiting Step

The gate-opening step in unliganded HCN2 has been shown to be a voltage-independent equilibrium: notably, the open probability reaches a limiting maximum value less than 100 % even at strong hyperpolarizations that should drive voltage-dependent equilibria maximally forward (Craven and Zagotta 2004). This limited open probability was apparent in the early phase of activation of HCN2 WT in our TEVC recordings (Online Resource 4): unliganded channels opened during the early phase to a maximum open probability less than one, before cAMP binding in the late phase led to further increases in open probability

(Wang et al. 2002). However, while this demonstrated the thermodynamic influence of the voltage-independent gate-opening step, our recordings found little evidence of a voltage-independent limit to activation kinetics at strong hyperpolarization. Instead, the value of τ_{early} continued to decrease with stronger hyperpolarizations for all the channels studied (Fig. 3 for HCN2 R591E and ΔαC, Fig. 4e for ΔCNB). This means that over a large voltage range, the voltage-independent gate-opening step of HCN2 channels must be rapidly equilibrating compared to the rate-limiting voltage-dependent steps that are presumed to involve inward S4 charge movement in all HCN channels (Männikkö et al. 2002; Bruening-Wright et al. 2007).

Since HCN2 R591E and ΔαC exhibited voltage-dependent τ_{early} values of 80–120 ms at −150 mV, we can infer the voltage-independent gate-opening step has a time constant not more than ~100 ms in these channels. A previous study (Wang et al. 2002) also failed to detect a plateau in the τ versus V relationship, but that study did not test voltages more than 25 mV negative of the $V_{1/2}$. Our observations extend to −150 mV, which in the case of ΔCNB is a full 70 mV more negative than $V_{1/2}$. While there are possibly multiple voltage-dependent steps in the activation pathway that are rate-limiting, our results show that a subset of such steps (i.e. at least one step) must be sensitive to the presence or absence of the quickening conformation: for concision in further discussion, we will refer to this key subset of voltage-dependent steps as the Quick-Activating (QA) steps. A quantitative indicator of voltage dependence in each derivative was calculated as the ratio of τ_{early} values for pairs of activation voltages spaced 20 mV apart, e.g. $\tau_{early(-130\ mV)}/\tau_{early(-150\ mV)}$ (Online Resource 7b). As hyperpolarization grew stronger, the voltage dependence did grow somewhat weaker (ratio values closer to unity), but even at the strongest hyperpolarization the ratio $\tau_{early(-130\ mV)}/\tau_{early(-150\ mV)}$ was >1.7 for both HCN2 R591E and ΔαC. The τ_{early} voltage-dependence ratios for ΔCNB were slightly lower than corresponding ratios for HCN2 R591E and ΔαC (significant, one-sided $p < 0.04$ for all comparisons) but were still well above unity.

Thus deletion of the CNB fold from an unliganded HCN channel can be understood to have different effects on different steps of the activation pathway. The voltage-independent gate-opening step likely has its equilibrium shifted towards the open state due to removal of autoinhibition, producing the positively shifted $V_{1/2}$. Quite possibly, the gate-opening step also has its rate increased in parallel with the thermodynamic effect, but this step is too fast to be rate-limiting for the overall activation rate. On the contrary, disruption of the quickening conformation in ΔCNB decreases the rate of one or more QA steps, producing slower voltage-dependent activation overall. This scenario can be contrasted with the "relief" of autoinhibition by a different means, that is, addition of cAMP to a channel with a complete CNB fold. The voltage-independent gate-opening step would be similarly shifted in thermodynamic terms, enabling higher maximal open probability and positively shifted $V_{1/2}$. But additionally, cAMP binding accelerates the QA steps with the quickening conformation always present; this effect might more properly be viewed as "enhancement" rather than "relieving autoinhibition", since the effect does not mimic the consequences of altogether removing the autoinhibitory CNB fold.

Deactivation is Slowed Down by cAMP Binding to an Intact CNB Fold More Than by Autoinhibition Relief Through CNB Fold Deletion

Another feature of the autoinhibition mechanism we wished to test was the speeding of deactivation, which has been reported to be more pronounced than effects on activation kinetics (DiFrancesco 1999). We tested deactivation using a protocol with a 3-s activation epoch at a strong hyperpolarization which should enable HCN2 WT channels to accumulate in the cAMP-liganded state before deactivation is tracked. We would thus expect that among our various derivatives, relief of autoinhibition as indicated by $V_{1/2}$ (ΔCNB or cAMP-liganded HCN2 WT) should be reliably associated with slower deactivation. Because the endpoint of deactivation transients was reliably achieved for all experiments, we measured deactivation using the parameter $t_{1/2}$ (time to reach midpoint of total decay amplitude); $t_{1/2}$ should take into account both the initial lag phase and the time for current decay.

Both HCN2 R591E and ΔαC both deactivated faster than HCN2 WT (Fig. 5a): at a fixed voltage of 0 mV, the mean $t_{1/2}$ values were 140 ± 22 ms ($n = 10$) and 170 ± 14 ms ($n = 10$) for HCN2 R591E and ΔαC, respectively, significantly faster than that of HCN2 WT (290 ± 58 ms, $n = 39$; one-sided $p < 10^{-6}$ for both comparisons with HCN2 WT). These findings confirm the well-known effect of cAMP to slow down deactivation. We considered that the $V_{1/2}$ of HCN2 WT was 15–17 mV more depolarized than that of other derivatives, indicating a weaker driving force for outward voltage-sensor movement in HCN2 WT at a fixed voltage. However, the weaker driving force cannot be the sole explanation for the slower deactivation of HCN2 WT: testing deactivation with greater driving force at +40 mV did accelerate HCN2 WT deactivation, but the effect was <1.4-fold and the kinetics still did not match the fast deactivation of the autoinhibited channels at 0 mV (Fig. 5b). Therefore, autoinhibition relief by cAMP binding has an effect on deactivation that is disproportionately large compared to its effect on $V_{1/2}$.

For the truncated ΔXC, which retains a CNB fold capable of mediating cAMP potentiation, slow deactivation

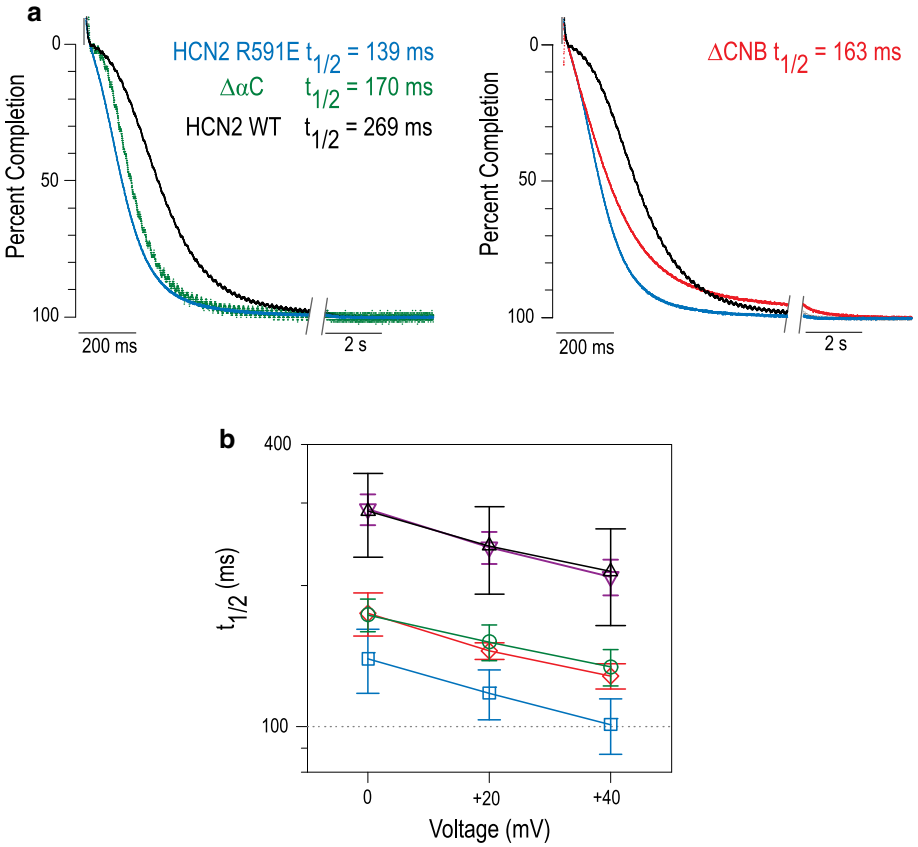

Fig. 5 cAMP-liganded HCN2 channels exhibit open-state trapping with slower deactivation compared to autoinhibited HCN2 derivatives and truncated ΔCNB. **a** Representative examples of deactivation currents at 0 mV, each normalised to total decay amplitude. Traces are from HCN2 WT (*black*) and HCN2 R591E (*blue*) in each panel, and ΔαC (*green*, *left panel*) and ΔCNB (*red*, *right panel*). Deactivation $t_{1/2}$ values for each example trace are indicated, with HCN2 R591E showing the smallest $t_{1/2}$ value. *Axis break* indicates change in plot timescale for clarity; no data were omitted. See Online Resource 8 for full deactivation protocol and traces at different voltages. **b** Mean $t_{1/2}$ values for all channels with *error bars* showing SD; for some channels the bars are drawn wider for clarity. Symbols are: HCN2 WT, *black up-triangles* with wider *error bars* (number of recordings $n = 39$); ΔXC, *purple down-triangles* ($n = 9$); HCN2 R591E, *blue squares* (n = 10); ΔαC, *green circles* ($n = 10$); ΔCNB, *red diamonds* with wider *error bars* ($n = 6$)

was observed matching HCN2 WT (Fig. 5b). In contrast ΔCNB, with autoinhibition constitutively relieved, did not deactivate slowly like cAMP-liganded HCN2 WT: ΔCNB deactivation kinetics were >1.7 fold faster than HCN2 WT at all voltages studied (significant, one-sided $p < 10^{-4}$; Fig. 5a-right, b). Thus, the slow deactivation characteristic of cAMP-liganded HCN2 WT requires not only relief of autoinhibition (successful in ΔCNB) but also requires an intact and cAMP-liganded CNB fold (unavailable to ΔCNB). This provides an example of "open state trapping" which has been observed in HCN4 derivatives (Wicks et al. 2009, 2011), similarly reliant on the presence of an intact CNB fold with bound cAMP. Open-state trapping illustrates well that the extent of autoinhibition as measured by $V_{1/2}$ alone is not a reliable predictor of deactivation kinetics. As with activation kinetics, it provides another case where "relief of autoinhibition" is not an apt description of the effect of cAMP binding.

Conversely, while the two autoinhibited derivatives HCN2 R591E and ΔαC had very similar $V_{1/2}$, they showed differences in deactivation kinetics. The deactivation $t_{1/2}$ values for ΔαC were slower than those of HCN2 R591E with a factor difference between 1.2 and 1.4 for voltages from 0 to +40 mV (Fig. 5b). This difference was less dramatic than was found for τ_{early} of activation (>1.5 fold for voltages from −90 to −150 mV) but it was statistically significant (one-sided $p < 0.002$) for all three voltages studied. Thus, of these two constitutively autoinhibited derivatives, the full length HCN2 R591E shows faster kinetics for both activation and deactivation.

Inhibition of HCN2 by PIP_2 Depletion Fails to Slow Down Activation Kinetics

The above work showed that the extent of autoinhibition as indicated by $V_{1/2}$ was a poor predictor of both activation

and deactivation kinetics. To test an example of HCN channel modulation that does not involve the CNB fold directly, we examined the effect of the lipid messenger phosphatidylinositol 4,5-bisphosphate (PIP_2). PIP_2 potentiates HCN channel activation producing depolarized $V_{1/2}$ values (Pian et al. 2006; Zolles et al. 2006). The binding sites for PIP_2 in the transmembrane and C-linker regions of HCN channels (Flynn and Zagotta 2011) are present in all the derivatives studied in this work. We tested whether PIP_2 depletion would slow activation kinetics of HCN2 WT in a fashion parallel to the hyperpolarization of $V_{1/2}$. We used Wortmannin, an inhibitor of phosphatidylinositol (PI) 4-kinase (Vanhaesebroeck et al. 2001), to decrease the available levels in the oocyte of phospho-PI derivatives including PIP_2 (Pian et al. 2006; Zolles et al. 2006).

HCN2 WT activation was tested in paired measurements made in the same oocyte before and after treatment with 45 μM Wortmannin (Fig. 6a). A negative shift in $V_{1/2}$ was observed with a mean $\Delta V_{1/2}$ of -16.6 ± 7.9 mV ($n = 11$) which was significantly different from zero (one-sided $p < 10^{-4}$), indicating a degree of gating inhibition similar to that observed in previous reports (Pian et al. 2006; Zolles et al. 2006). Notably, the $\Delta V_{1/2}$ from depletion of phospho-PI derivatives was similar in magnitude to the hyperpolarizing shift in $V_{1/2}$ observed from eliminating cAMP binding (HCN2 R591E or ΔαC vs. HCN2, difference of 16–18 mV in mean $V_{1/2}$). In analogous treatment with bath solutions containing the vehicle solvent DMSO without Wortmannin, the mean $V_{1/2}$ shift was not significantly different from zero ($\Delta V_{1/2} = -3.0 \pm 7.9$ mV, $n = 11$, two-sided $p > 0.2$).

Although Wortmannin treatment clearly inhibited gating, there was no statistically significant increase in τ_{early} or lag duration d at all voltages studied (one-sided $p > 0.06$; Fig. 6b left panel) with the exception of a 10 % increase in d at −150 mV (significant, one-sided $p < 0.03$); in fact, for −90 mV there was a slight reduction in mean τ_{early}. We confirmed the same lack of effect on activation kinetics in ΔαC where cAMP binding would not be a factor. Wortmannin treatment hyperpolarized the $V_{1/2}$ of ΔαC, albeit to a lesser extent than seen in HCN2 WT (mean $\Delta V_{1/2}$ for ΔαC, -4.8 ± 2.5 mV, $n = 4$; significantly different from zero, one-sided $p < 0.02$). Just as for HCN2 WT, there was no associated significant increase in τ_{early} or d over all voltages studied (one-sided $p > 0.1$; Fig. 6b-right panel) with the exception of a 9 % increase in τ_{early} at −130 mV (significant, one-sided $p < 0.02$).

Notably, transients at each test voltage had a similar shape before and after Wortmannin treatment (Fig. 6c–f), and in fact were visually indistinguishable (superimposable) after being scaled to the absolute transient amplitude. This was true even at weak hyperpolarizations near the $V_{1/2}$ value, where the total amplitude of the 3-s activation transient was reduced substantially upon Wortmannin treatment, leading to hyperpolarized $V_{1/2}$. This is consistent with a scenario where any steps influenced by PIP_2 are rapidly equilibrating (not rate-limiting); those steps would have equilibrium shifted towards the reverse direction, resulting in a hyperpolarizing shift of $V_{1/2}$ without altering the activation kinetics. Moreover, quite obviously the negligible effect of PIP_2 depletion on activation kinetics of full length HCN2 is distinct from the slowing of activation kinetics resulting from removal of the quickening conformation to produce ΔCNB.

Discussion

Insufficiency of Simple Autoinhibition Model Based on $V_{1/2}$ Assessment

Consequences for HCN channel modulation from truncations of the C-terminal region are likely to have physiological relevance, since C-terminal truncations have been identified in human patients with cardiac sinus node defects (Schulze-Bahr et al. 2003; Schweizer et al. 2010) and even in myocardial tissues of healthy mice (Ye and Nerbonne 2009). Thus, it is essential to generate a cohesive biophysical theory of how the molecular structure can determine kinetic properties. While the autoinhibition model has provided a valuable organising framework for understanding the mechanistic consequences of C-terminal truncation, our results show the limits of the simplest form of this model in regards to predicting activation speeds.

The most important mechanistic insights from our findings are that (a) for activation kinetics in particular, there is a quickening effect derived from having a CNB fold which works in opposition to the hyperpolarization of $V_{1/2}$ mediated by the autoinhibition mechanism, and (b) overall the presence or absence of a full-length CNB fold including helix αC is a more important determinant of kinetics than the presence or absence of autoinhibition. Unexpectedly, we found that an autoinhibited derivative activates faster than a derivative with autoinhibition fully abolished by CNB fold deletion (HCN2 R591E activates faster than ΔCNB). Among the five channels studied, the presence of a full-length CNB fold was associated with a faster early phase of activation compared to channels whose CNB fold was partial or missing; this held whether or not the full-length CNB fold was capable of binding endogenous cAMP to relieve autoinhibition during a later phase of activation. We propose that the presence of a full-length CNB fold ensures the preservation of a "quickening conformation" required for fast activation kinetics. Deletion of the extreme-C region is tolerated, but deletion of the helix αC or the entire CNB fold compromises the

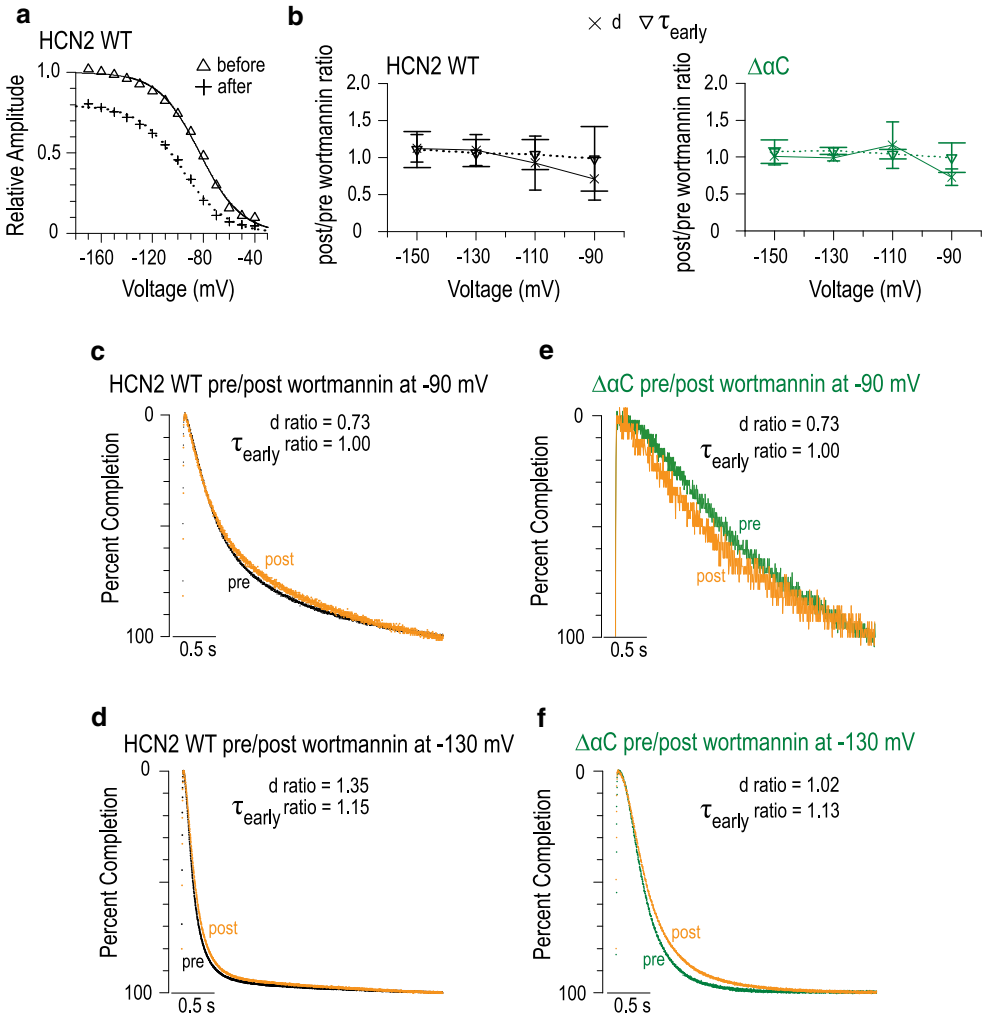

Fig. 6 Treatment with Wortmannin to deplete PIP_2 results in hyperpolarization of $V_{1/2}$ without slowing of activation kinetics. **a** Conductance–voltage relation for an example oocyte expressing HCN2 WT before and after treatment with PIP_2. See Online Resource 9 for full traces. Boltzmann equation fit parameters were $V_{1/2} = -83.0$ mV, $s = 16.2$ mV before Wortmannin, and $V_{1/2} = -96.8$ mV, $s = 17.2$ mV after Wortmannin ($\Delta V_{1/2} = -13.8$ mV). **b** *Points* plot mean Wortmannin effects for τ_{early} and d for HCN2 WT and ΔαC at different voltages. Effect on a parameter is calculated as the ratio of the value after Wortmannin treatment to the value before treatment. *Error bars* show SD, with bars for d drawn wider for clarity; number of paired recordings $n = 11$ for HCN2 WT and $n = 4$ for ΔαC, except one recording ΔαC at −90 mV was excluded because its amplitude was <60 nA. **c–f** Superimpositions of normalised example transients before and after Wortmannin treatment, for channels and voltages as marked, with Wortmannin effects for τ_{early} and d indicated. HCN2 WT examples are from the oocyte in panel **a**; ΔαC examples are from an oocyte where the shift in $V_{1/2}$ due to Wortmannin treatment was $\Delta V_{1/2} = -6.7$ mV

quickening conformation resulting in slower activation. For deactivation kinetics, we found HCN2 WT with cAMP bound exhibits slower deactivation than the autoinhibition-free ΔCNB, providing another example of the "open-state trapping" effect (Wicks et al. 2009, 2011) first seen in HCN4 channels containing an S4 mutation. Thus, while $V_{1/2}$ is typically taken as the primary indicator of the inhibition status, it fails to correlate in a general fashion with either activation kinetics or deactivation kinetics, so that even derivatives with similar $V_{1/2}$ due to equivalent strength of constitutive autoinhibition can exhibit different kinetics (ΔαC kinetics are slower than HCN2 R591E for both activation and deactivation).

Imagining the minimal voltage-gating unit to consist of an HCN channel truncated to remove the CNB fold, the autoinhibition theory envisions addition of the C-terminal region as introduction of a repressive straining element disfavouring the activated open state. However, our work shows this view holds reliably only in thermodynamic terms for the voltage-independent gate-opening step: for activation kinetics, addition of an unliganded C-terminal region actually speeds up the voltage-dependent "Quick-

Activating" (QA) step that is rate-limiting. Consequently, for voltage-dependent activation and deactivation kinetics, cAMP binding to the C-terminal region enables the formation of new channel structures that kinetically favour the open state (faster activation and slower deactivation) beyond what could be achieved by the minimal unit.

Importance of a Complete CNB Fold

The CNB fold is not believed to be proximal to the transmembrane region which presumably controls voltage-dependent channel gating (Zagotta et al. 2003), so how might the CNB fold form a structural requirement for the "quickening conformation" enabling fast kinetics? It is probable that at least one of the elements involved in the quickening conformation is the C-linker immediately N-terminal to the CNB fold. The C-linker has been proposed to influence gating in two ways. First, the C-linker is directly connected to the S6 gate that regulates pore opening, and changes in intersubunit interactions governing C-linker self-association have been proposed to alter S6 orientation (Craven and Zagotta 2004; Zhou et al. 2004; Lolicato et al. 2011; Wu et al. 2012). Second, the C-linker has been proposed to interact directly with the S4–S5 linker that transduces S4 movement to pore gate-opening (Decher et al. 2004; Prole and Yellen 2006; Kwan et al. 2012). Thus, the conformation and orientation of the four C-linkers within the tetramer can potentially influence both the voltage-independent gate-opening step and voltage-dependent steps such as the QA step.

Although many mechanisms are possible, we can propose a simple model for the structural effects of CNB fold truncation, where the rate of S4 movement in the QA step is sensitive to the relative orientation of the C-linker between neighbouring subunits. See Fig. 7 for a schematic showing a hindering C-linker conformation (shown as wavy block) that slows down activation; this conformation can be avoided given the correct "quickening" conformation of the CNB fold (shown as horseshoe, Fig. 7 first row). Even though the helix αC is not in direct contact with the C-linker, it is quite plausibly important for maintaining C-linker orientation, because intersubunit self-association interactions have been demonstrated (Matulef and Zagotta, 2002) for the helix αC in cyclic nucleotide-gated channels (homologues of HCN channels). Loss of the helix αC to produce ΔαC (Fig. 7 second row) preserves the straining structures critical for autoinhibition within the remaining portion of the C-terminal region, but might also re-orient that region; this reorientation mildly disrupts the quickening conformation which slows down the rate-limiting QA step. A more dramatic loss of the entire CNB fold to produce ΔCNB (Fig. 7 third row) eliminates critical C-linker-CNB fold contacts; this could create a more dramatic disruption of the quickening conformation so that activation becomes slower than in HCN2 R591E. At the same time, removal of the straining structure responsible for autoinhibition would thermodynamically enhance the voltage-independent gate-opening step (giving depolarized $V_{1/2}$ values) and might even speed up this step, but this step would not be rate-limiting in ΔCNB.

Comparison of TEVC Results with Previous Excised Patch Studies

Our study focuses on how the cytoplasmic CNB fold influences activation when it is unliganded, in contrast with numerous previous studies focused on understanding the cAMP regulation mechanism. Typical studies of cAMP regulation in HCN channels control the cAMP concentration using either the inside-out excised patch configuration (DiFrancesco and Tortora 1991; Gauss et al. 1998; Ludwig et al. 1998; Santoro et al. 1998; DiFrancesco 1999; Wainger et al. 2001) or "whole-cell" patch-clamp of small mammalian cells (Qu et al. 2001), where cellular components are exchanged with the contents of the bath (excised patch) or pipette lumen (whole-cell). One consequence of losing cellular components is a "rundown" suppression of HCN channel activity (DiFrancesco et al. 1986), most prominently including a hyperpolarization of the $V_{1/2}$ that has been shown to be caused by PIP_2 depletion (Pian et al. 2006; Zolles et al. 2006). The truncated HCN2 derivatives ΔCNB and ΔαC were first characterised in excised patch studies which were essential for establishing the autoinhibition model of cAMP regulation (Wainger et al. 2001); our study is the first to describe the kinetics of these truncation derivatives in intact oocytes before rundown has occurred.

A dramatic slowing of activation kinetics is another feature of rundown (DiFrancesco et al. 1986) that at first glance seems to parallel the hyperpolarization of the $V_{1/2}$. However, our findings show the slowing effect is in fact unlikely to be due to PIP_2 depletion like the $V_{1/2}$ shift, since even a 20 mV hyperpolarizing shift in $V_{1/2}$ induced by Wortmannin did not significantly slow down the early phase of activation of HCN2 WT. Our findings complement those of a previous study where PIP_2 derivatives were added back to unliganded HCN2 in excised patches after rundown had occurred: a positive $V_{1/2}$ shift was obtained without accelerating activation kinetics (Pian et al. 2006). Thus, the slowing of activation during rundown is most likely due to a modulatory factor distinct from PI derivatives like PIP_2.

There are two aspects of gating behaviour observed in our TEVC findings which differ from behaviour in previous excised patch experiments on the same channels; these differences suggest additional influences of cellular factors lost during rundown in the excised patch experiments. One

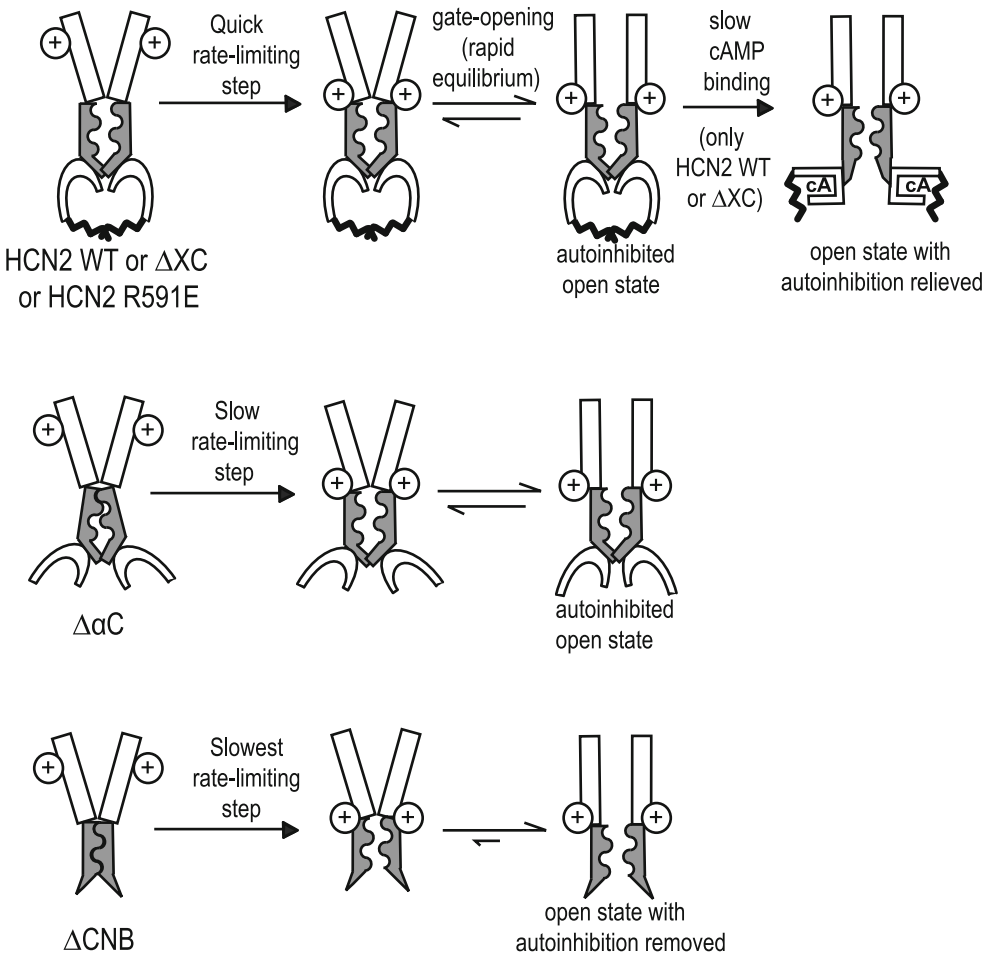

Fig. 7 Schematic summarising how a deleterious conformation hindering activation could be avoided through the presence of the helix αC in the CNB fold, independent of the autoinhibition mechanism. Schematics show participating elements conceptually and are not intended to depict detailed structures. Two of four subunits are depicted with transmembrane domains shown as *tilted rectangles*. The QA step that is rate-limiting for activation involves hyperpolarization-dependent inward movement of S4 voltage-sensor (*circle* with *plus sign*), whereas the step that opens the S6 gate (reorientation of *rectangles*) is voltage-independent and rapidly equilibrating relative to the QA step; the pathway contains multiple other steps which are omitted. The C-terminal region is shown with C-linker (*wavy block*), cAMP binding site (*horseshoe*) and helix αC (*zigzag*); extreme-C region and tetramerization interactions of the transmembrane and C-linker regions are omitted. Differently truncated HCN channels have an intact CNB fold (*first row*) which is unliganded in intact oocytes before hyperpolarization, or a CNB fold truncated before the helix αC (*second row*), or no CNB fold (*third row*). The gate-opening step is thermodynamically disfavoured by CNB-dependent autoinhibition (*first* and *second rows*). However, the presence of the helix αC (only *first row*) maintains the quickening conformation required for the channel to quickly proceed through the rate-limiting QA step. In channels missing helix αC (*second* and *third rows*) the C-linker enters an alternative "hindering" arrangement producing slow activation

difference concerns the detection of the voltage-independent gate-opening step; the other difference concerns the relative activation rates of uninhibited ΔCNB versus autoinhibited channels like HCN2 R591E and ΔαC. Closer examination shows that our TEVC experiments do not contradict the previous findings derived from excised patches, but rather provide more detail on relevant mechanistic steps, specifically regarding their operating rates in an intact cell and their susceptibility to rundown.

The voltage-independent gate-opening step is one example of a mechanistic step slowed by rundown: in intact oocytes, we found its time constant was shorter than ~100 ms in unliganded full-length channels (HCN2 R591E or HCN2 WT τ_{early}), whereas it was ~500 ms in unliganded HCN2 WT in excised patches after rundown (Chen et al. 2007). The voltage-dependent QA step also appears to be slowed by rundown, such that in excised patches, time constants were in excess of 1500 ms for hyperpolarizations weaker than −130 mV (Chen et al. 2007). We note that rundown appears to slow down the gate-opening step preferentially over the QA step: in intact oocytes, the voltage-independent gate-opening step remains rapidly equilibrating

compared to voltage-dependent steps even at 50 to 70 mV negative of $V_{1/2}$, whereas in excised patches after rundown, the voltage-independent gate-opening step became rate-limiting at only 30 mV negative of $V_{1/2}$ (Chen et al. 2007). This illustrates how in principle, different mechanistic steps can show different sensitivities to different cellular factors.

In intact oocytes, HCN2 R591E (autoinhibition imposed) showed faster activation than ΔCNB (autoinhibition removed); this is a reversed relationship to that found in excised patches (Wainger et al. 2001). This suggests that rundown affects the two derivatives differently. To be specific, we propose that the loss of cellular factors during excised patch rundown could cause a disproportionately large slowing effect on activation of HCN2 R591E and unliganded HCN2 WT, in comparison with ΔCNB where the slowing effect would be slight or none. Then excised patch measurements could show ΔCNB had faster kinetics than the full length constructs. Therefore, taking our new findings with the previous excised patch results together, we propose that the activation pathways of HCN2 R591E and ΔCNB have different rate-limiting steps. The voltage-dependent QA step that is rate-limiting for HCN2 R591E in intact oocytes is strongly sensitive to rundown in excised patches, whereas a distinct step whose forward rate is most severely compromised by CNB deletion is rundown-insensitive. The requirement of the QA step for a cellular factor (distinct from PIP_2) would be in addition to the requirement for the quickening conformation. Thus, the cellular factor modulating the QA step might in fact still bind properly to ΔCNB or other truncated channels, but its presence would no longer be sufficient to preserve fast kinetics in those mutant channels due to lack of the quickening conformation.

We do not exclude the possibility that the observed TEVC versus excised patch differences arise from other factors like bath solutions or even protein biogenesis. However, any such responsible factor apparently acts differently on ΔCNB than it acts on longer channels like HCN2 R591E, ΔXC or HCN2 WT, and, moreover, acts differently on the voltage-dependent QA step than on the voltage-independent gate-opening step.

Outlook

Our results show that the structural basis of the activation kinetics of an unliganded HCN channel must be considered separately from the basis of the $V_{1/2}$ value. In this work, we have systematically described a well-defined effect on activation kinetics of the HCN2 homomeric channel due to well-defined truncations; this effect is not predictable from the existing autoinhibition theory. Paradoxically, an intact CNB fold is autoinhibitory for gate-opening yet is important for ensuring a quickening conformation producing efficient kinetics of S4 movement in the rate-limiting QA step. The quickening conformation mechanism may apply to various HCN subtypes due to the strong conservation of the key structures of the CNB fold and C-linker, in contrast with the poorly conserved extreme-C region which is inessential for the quickening conformation. However, the quantitative effect of the quickening conformation may be different among subtypes, as is the case with other CNB-fold-dependent mechanisms like autoinhibition and cAMP-dependent relief (Wainger et al. 2001; Vemana et al. 2004) and open-state trapping (Wicks et al. 2011).

Besides variations in subunit composition, variations in levels of cellular factors are a potential source of tissue-specific functional diversity in I_h. This highlights the importance of the possibility that a cellular factor distinct from cAMP and PIP_2 is necessary (but not sufficient) for preservation of the quickening conformation. Although the search for a cellular factor will require substantial investigation, measuring the speed of the rate-limiting QA step could provide a valuable experimental test for verifying the functional effect of any candidate factors.

Truncations of HCN4 have been reported in sinus bradycardia patients exhibiting abnormally low heart rate even at resting conditions (Schulze-Bahr et al. 2003; Schweizer et al. 2010). A full understanding of I_h kinetics in such patients can potentially benefit from better understanding of the relative orientation of cytoplasmic C-terminal regions in heteromeric HCN channels containing truncated subunits, within the context of an intact cell. Autoinhibition might be preserved or abolished depending on the presence of the N-terminal region of the CNB fold and on the number and placement of truncated subunits within the heterotetramer, but the most likely primary effect on S4 movement would be deceleration due to disruption of the quickening conformation. This would apply whether or not PIP_2 potentiation was disrupted. And it would also apply even with basal concentrations of cAMP, where most HCN channels have their CNB folds unliganded. Thus, identifying the structural elements of the quickening conformation producing faster I_h activation may prove important in predicting and managing phenotypes of cardiopathies.

Acknowledgments This work was supported by grants from the Natural Sciences and Engineering Research Council to E. C. Y. (Discovery Grant 312124) and to K. E. A. M. (CGS-M Graduate Scholarship), and a Career Investigator (Scholar) Award to E. C. Y. from the Michael Smith Foundation for Health Research. We thank S. A. Siegelbaum for the donation of HCN2 WT, HCN2 R591E and ΔCNB; S. J. Saad for help with sequencing and preliminary recordings; T. W. Claydon and D. A. Page for comments on the manuscript; and all members of the Young lab for helpful discussions and technical support.

Conflict of interest The authors declare that they have no conflict of interest.

Ethical Standard All applicable international, national, and institutional guidelines were followed for the care and use of animals and for all procedures involving animals, in accordance with the ethical standards of Simon Fraser University.

References

Akimoto M, Zhang Z, Boulton S, Selvaratnam R, VanSchouwen B, Gloyd M, Accili EA, Lange OF, Melacini G (2014) A mechanism for the auto-inhibition of hyperpolarization-activated cyclic nucleotide-gated (HCN) channel opening and its relief by cAMP. J Biol Chem 289:22205–22220

Altomare C, Bucchi A, Camatini E, Baruscotti M, Viscomi C, Moroni A, DiFrancesco D (2001) Integrated allosteric model of voltage gating of HCN channels. J Gen Physiol 117:519–532

Barbuti A, Baruscotti M, Altomare C, Moroni A, DiFrancesco D (1999) Action of internal pronase on the f-channel kinetics in the rabbit SA node. J Physiol 520(Pt 3):737–744

Bell DC, Yao H, Saenger RC, Riley JH, Siegelbaum SA (2004) Changes in local S4 environment provide a voltage-sensing mechanism for mammalian hyperpolarization-activated HCN channels. J Gen Physiol 123:5–19

Benarroch EE (2013) HCN channels: function and clinical implications. Neurology 80:304–310

Biel M, Wahl-Schott C, Michalakis S, Zong X (2009) Hyperpolarization-activated cation channels: from genes to function. Physiol Rev 89:847–885

Bruening-Wright A, Larsson HP (2007) Slow conformational changes of the voltage sensor during the mode shift in hyperpolarization-activated cyclic-nucleotide-gated channels. J Neurosci 27:270–278

Bruening-Wright A, Elinder F, Larsson HP (2007) Kinetic relationship between the voltage sensor and the activation gate in spHCN channels. J Gen Physiol 130:71–81

Chen J, Mitcheson JS, Lin M, Sanguinetti MC (2000) Functional roles of charged residues in the putative voltage sensor of the HCN2 pacemaker channel. J Biol Chem 275:36465–36471

Chen S, Wang J, Siegelbaum SA (2001) Properties of hyperpolarization-activated pacemaker current defined by coassembly of HCN1 and HCN2 subunits and basal modulation by cyclic nucleotide. J Gen Physiol 117:491–504

Chen S, Wang J, Zhou L, George MS, Siegelbaum SA (2007) Voltage sensor movement and cAMP binding allosterically regulate an inherently voltage-independent closed-open transition in HCN channels. J Gen Physiol 129:175–188

Chow SS, Van Petegem F, Accili EA (2012) Energetics of cyclic AMP binding to HCN channel C terminus reveal negative cooperativity. J Biol Chem 287:600–606

Craven KB, Zagotta WN (2004) Salt bridges and gating in the COOH-terminal region of HCN2 and CNGA1 channels. J Gen Physiol 124:663–677

Craven KB, Olivier NB, Zagotta WN (2008) C-terminal movement during gating in cyclic nucleotide-modulated channels. J Biol Chem 283:14728–14738

Decher N, Chen J, Sanguinetti MC (2004) Voltage-dependent gating of hyperpolarization-activated, cyclic nucleotide-gated pacemaker channels: molecular coupling between the S4-S5 and C-linkers. J Biol Chem 279:13859–13865

DiFrancesco D (1999) Dual allosteric modulation of pacemaker (f) channels by cAMP and voltage in rabbit SA node. J Physiol 515:367–376

DiFrancesco D, Tortora P (1991) Direct activation of cardiac pacemaker channels by intracellular cyclic AMP. Nature 351:145–147

DiFrancesco D, Tromba C (1988) Muscarinic control of the hyperpolarization-activated current (i_f) in rabbit sino-atrial node myocytes. J Physiol 405:493–510

DiFrancesco D, Ferroni A, Mazzanti M, Tromba C (1986) Properties of the hyperpolarizing-activated current (i_f) in cells isolated from the rabbit sino-atrial node. J Physiol 377:61–88

Elinder F, Männikkö R, Pandey S, Larsson HP (2006) Mode shifts in the voltage gating of the mouse and human HCN2 and HCN4 channels. J Physiol 575:417–431

Flynn GE, Zagotta WN (2003) A cysteine scan of the inner vestibule of cyclic nucleotide-gated channels reveals architecture and rearrangement of the pore. J Gen Physiol 121:563–582

Flynn GE, Zagotta WN (2011) Molecular mechanism underlying phosphatidylinositol 4,5-bisphosphate-induced inhibition of SpIH channels. J Biol Chem 286:15535–15542

Gauss R, Seifert R, Kaupp UB (1998) Molecular identification of a hyperpolarization-activated channel in sea urchin sperm. Nature 393:583–587

Jiang Y-Q, Sun Q, Tu H-Y, Wan Y (2008) Characteristics of HCN channels and their participation in neuropathic pain. Neurochem Res 33:1979–1989

Kaupp UB, Seifert R (2001) Molecular diversity of pacemaker ion channels. Annu Rev Physiol 63:235–257

Kwan DC, Prole DL, Yellen G (2012) Structural changes during HCN channel gating defined by high affinity metal bridges. J Gen Physiol 140:279–291

Liman ER, Tytgat J, Hess P (1992) Subunit stoichiometry of a mammalian K^+ channel determined by construction of multimeric cDNAs. Neuron 9:861–871

Lolicato M, Nardini M, Gazzarrini S, Möller S, Bertinetti D, Herberg FW, Bolognesi M, Martin H, Fasolini M, Bertrand JA et al (2011) Tetramerization dynamics of C-terminal domain underlies isoform-specific cAMP gating in hyperpolarization-activated cyclic nucleotide-gated channels. J Biol Chem 286:44811–44820

Ludwig A, Zong X, Jeglitsch M, Hofmann F, Biel M (1998) A family of hyperpolarization-activated mammalian cation channels. Nature 393:587–591

Lüthi A, McCormick DA (1998) H-Current: properties of a neuronal and network pacemaker. Neuron 21:9–12

Mangoni ME, Nargeot J (2008) Genesis and regulation of the heart automaticity. Physiol Rev 88:919–982

Männikkö R, Elinder F, Larsson HP (2002) Voltage-sensing mechanism is conserved among ion channels gated by opposite voltages. Nature 419:837–841

Männikkö R, Pandey S, Larsson HP, Elinder F (2005) Hysteresis in the voltage dependence of HCN channels: conversion between two modes affects pacemaker properties. J Gen Physiol 125:305–326

Matulef K, Zagotta WN (2002) Multimerization of the ligand binding domains of cyclic nucleotide-gated channels. Neuron 36:93–103

Noam Y, Bernard C, Baram TZ (2011) Towards an integrated view of HCN channel role in epilepsy. Curr Opin Neurobiol 21:873–879

Pian P, Bucchi A, Robinson RB, Siegelbaum SA (2006) Regulation of gating and rundown of HCN hyperpolarization-activated channels by exogenous and endogenous PIP_2. J Gen Physiol 128:593–604

Proenza C, Angoli D, Agranovich E, Macri V, Accili EA (2002) Pacemaker channels produce an instantaneous current. J Biol Chem 277:5101–5109

Prole DL, Yellen G (2006) Reversal of HCN channel voltage dependence via bridging of the S4-S5 linker and Post-S6. J Gen Physiol 128:273–282

Puljung MC, DeBerg HA, Zagotta WN, Stoll S (2014) Double electron-electron resonance reveals cAMP-induced conformational change in HCN channels. Proc Natl Acad Sci USA 111:9816–9821

Qu J, Barbuti A, Protas L, Santoro B, Cohen IS, Robinson RB (2001) HCN2 overexpression in newborn and adult ventricular myocytes: distinct effects on gating and excitability. Circ Res 89:E8–E14

Robinson RB, Siegelbaum SA (2003) Hyperpolarization-activated cation currents: from molecules to physiological function. Annu Rev Physiol 65:453–480

Rothberg BS, Shin KS, Phale PS, Yellen G (2002) Voltage-controlled gating at the intracellular entrance to a hyperpolarization-activated cation channel. J Gen Physiol 119:83–91

Santoro B, Liu DT, Yao H, Bartsch D, Kandel ER, Siegelbaum SA, Tibbs GR (1998) Identification of a gene encoding a hyperpolarization-activated pacemaker channel of brain. Cell 93:717–729

Santoro B, Chen S, Luthi A, Pavlidis P, Shumyatsky GP, Tibbs GR, Siegelbaum SA (2000) Molecular and functional heterogeneity of hyperpolarization-activated pacemaker channels in the mouse CNS. J Neurosci 20:5264–5275

Schulze-Bahr E, Neu A, Friederich P, Kaupp UB, Breithardt G, Pongs O, Isbrandt D (2003) Pacemaker channel dysfunction in a patient with sinus node disease. J Clin Invest 111:1537–1545

Schweizer PA, Duhme N, Thomas D, Becker R, Zehelein J, Draguhn A, Bruehl C, Katus HA, Koenen M (2010) cAMP sensitivity of HCN pacemaker channels determines basal heart rate but is not critical for autonomic rate control. Circ Arrhythm Electrophysiol 3:542–552

Stieber J, Hofmann F, Ludwig A (2004) Pacemaker channels and sinus node arrhythmia. Trends Cardiovasc Med 14:23–28

Vanhaesebroeck B, Leevers SJ, Ahmadi K, Timms J, Katso R, Driscoll PC, Woscholski R, Parker PJ, Waterfield MD (2001) Synthesis and function of 3-phosphorylated inositol lipids. Annu Rev Biochem 70:535–602

Vemana S, Pandey S, Larsson HP (2004) S4 movement in a mammalian HCN channel. J Gen Physiol 123:21–32

Wainger BJ, DeGennaro M, Santoro B, Siegelbaum SA, Tibbs GR (2001) Molecular mechanism of cAMP modulation of HCN pacemaker channels. Nature 411:805–810

Wang J, Chen S, Nolan MF, Siegelbaum SA (2002) Activity-dependent regulation of HCN pacemaker channels by cyclic AMP: signaling through dynamic allosteric coupling. Neuron 36:451–461

Wicks NL, Chan KS, Madden Z, Santoro B, Young EC (2009) Sensitivity of HCN channel deactivation to cAMP is amplified by an S4 mutation combined with activation mode shift. Pflugers Arch 458:877–889

Wicks NL, Wong T, Sun J, Madden Z, Young EC (2011) Cytoplasmic cAMP-sensing domain of hyperpolarization-activated cation (HCN) channels uses two structurally distinct mechanisms to regulate voltage gating. Proc Natl Acad Sci USA 108:609–614

Wu S, Gao W, Xie C, Xu X, Vorvis C, Marni F, Hackett AR, Liu Q, Zhou L (2012) Inner activation gate in S6 contributes to the state-dependent binding of cAMP in full-length HCN2 channel. J Gen Physiol 140:29–39

Ye B, Nerbonne JM (2009) Proteolytic processing of HCN2 and co-assembly with HCN4 in the generation of cardiac pacemaker channels. J Biol Chem 284:25553–25559

Zagotta WN, Olivier NB, Black KD, Young EC, Olson R, Gouaux E (2003) Structural basis for modulation and agonist specificity of HCN pacemaker channels. Nature 425:200–205

Zhou L, Siegelbaum SA (2007) Gating of HCN channels by cyclic nucleotides: residue contacts that underlie ligand binding, selectivity, and efficacy. Structure 15:655–670

Zhou L, Olivier NB, Yao H, Young EC, Siegelbaum SA (2004) A conserved tripeptide in CNG and HCN channels regulates ligand gating by controlling C-terminal oligomerization. Neuron 44:823–834

Zolles G, Klöcker N, Wenzel D, Weisser-Thomas J, Fleischmann BK, Roeper J, Fakler B (2006) Pacemaking by HCN channels requires interaction with phosphoinositides. Neuron 52: 1027–1036